# Stimulated Raman Imaging Below the Diffraction Limit with a MHz Laser

Christian T. Graefe, David Punihaole, Michael J. Lynch,

W. Ruchira Silva, and Renee R. Frontiera*

Department of Chemistry, University of Minnesota, Minneapolis, MN 55455

*To whom correspondence should be addressed: rrf@umn.edu

**Abstract**

Super-resolution techniques based on Raman spectroscopy could be implemented as label-free alternatives to fluorescence-based techniques due to their chemically specific signal and multiplexing potential. In previous work, we developed a stimulated Raman-based imaging technique that surpassed the diffraction limit using a toroidally-shaped pulse to deplete the signal in a spatially defined area. The photophysical principles of depletion and improved spatial resolution were demonstrated using a 1 kHz laser with high peak power that were able to efficiently drive depletion. However, this laser was not well-suited for soft matter samples, which degraded under the intense beams. To improve the biological capabilities of our setup, we have adapted our technique for a 2.04 MHz laser system. The increased repetition rate produces far more spectra per second, allowing us to decrease the pulse powers while maintaining reasonable acquisition times. Using the 2.04 MHz laser, we are able to demonstrate strong signal depletion of 62% and resolution enhancements of 52%, which is comparable to the metrics obtained with the 1 kHz laser. However, further improvements in resolution were not achieved despite increases in the depletion beam energy relative to the other beams. Frequency resolved optical gating analysis of the fundamental output of the 2.04 MHz laser indicated an inconsistent pulse phase and duration. We expect the inconsistent depletion was a result of this pulse profile and conclude that efficient depletion depends on highly reproducible and stable laser pulses.

**Keywords:** Super-resolution Raman microscopy, Sub-diffraction Raman imaging, Stimulated Raman microscopy, High repetition rate stimulated Raman spectroscopy

## Introduction

Super-resolution fluorescence microscopy techniques, such as stimulated emission depletion (STED),[1] photoactivated localization microscopy (PALM),[2] and stochastic optical reconstruction microscopy (STORM),[3] have revolutionized the field of optical imaging, allowing researchers to observe dynamic and structural details on unprecedentedly small length scales formerly inaccessible with conventional techniques. Prior to the development of super-resolution techniques, spatial resolution with optical techniques was thought to be limited to several hundred nanometers at best due to the diffraction limit.[4] The ability to elucidate nanoscale structural details has led to breakthroughs in numerous fields, particularly biophysics.[5–8] For example, super-resolution made the discovery of the membrane-associated periodic skeleton in neurons possible[9] and helped to clarify the role of mitochondria in apoptosis.[5,10–12]

Super-resolution fluorescence techniques, which break the optical diffraction limit through the use of spatially shaped beams or stochastically activated photoswitchable fluorophores, have several inherent disadvantages that can limit their applicability. Typically, the fluorescent proteins or dye molecules used as labels are large and bulky relative to the resolution length scales. These fluorophores can disrupt the structure or dynamics of the system of interest.[13,14] Additionally, fluorophores are susceptible to photobleaching, leading to a loss in signal and making quantitation difficult.[15,16] This is especially a concern for super-resolution techniques as they require high laser power densities, which increases the likelihood of photobleaching. There is also evidence to suggest that increased irradiance in live cell samples can alter cellular processes including

metabolism and proliferation, and can even lead to higher levels of phototoxicity.[17] Finally, since each analyte must be tagged with a fluorophore having a distinct emission profile, multiplex detection possibilities are limited. Since most emission profiles have rather broad bandwidths and numerous biorthogonal labeling steps can be complex, fluorescence microscopy techniques typically have practical limits of approximately five analytes without the use of complicated equipment and signal processing.[18,19]

To avoid the use of fluorophores, label-free super-resolution techniques have been the focus of significant research efforts.[4,20–34] Techniques based on Raman spectroscopy have drawn interest due to the fact that it probes vibrational modes that are inherent in a given molecule. Even if an analyte of interest has a Raman spectrum that makes it difficult to isolate in a matrix containing similar vibrations, a very small vibrational tag can be used to provide contrast. Raman tags include nitriles, alkynes, BH stretches, and CD stretches, which are all on the Å length scale.[35,36] These tags have a drastically lower probability of perturbing the system of interest than fluorophores, which are typically on the 1 nm length scale for organic dye molecules and the 10 nm length scale for fluorescent proteins. Additionally, Raman spectra contain information about the surrounding chemical environment,[37–42] and offer improved multiplexing capabilities due the peaks' narrow bandwidth when compared to fluorescence peaks.[43]

However, since Raman scattering is a weak process, standard Raman microscopy has limited use as a biological imaging technique. Stimulated Raman spectroscopy (SRS) is a type of Raman spectroscopy that uses two beams, a pump and a probe (which is sometimes called the Stokes beam), to increase the likelihood of a Raman transition occurring, thereby amplifying the signal.[44] The difference in energy between the pump and probe is equal to the energy of the vibration. SRS has gained popularity in biological imaging due to this enhancement beyond

standard Raman spectroscopy.[35,45–48] SRS imaging is well-established at MHz repetition rates, but has not been previously applied for super-resolution Raman measurements.

We have developed a super-resolution technique based on SRS in an attempt to attain nanoscale resolution without the need for fluorophores. In addition to the two Raman pulses used to generate SRS signal, we add a toroidally-shaped pulse to deplete the signal in a spatially defined area, similar to the idea behind the fluorescence-based technique STED. Previously, we demonstrated the photophysical principals behind this technique, including the depletion efficiency as a function of depletion beam polarization, timing, and power. We also achieved sub-diffraction limit spatial resolution.[20] As in STED and similar saturation-based techniques,[49] the depletion efficiency is crucially important to achieving sub-diffraction resolution, as the resolution depends nonlinearly on the saturation, according to the following equation:

$$\Delta r = \frac{\lambda}{2\pi sin\alpha \sqrt{1 + \frac{I_{MAX}}{I_{SAT}}}}$$

where $\Delta r$ is the full with at half maximum of the focal spot, $\lambda$ is the wavelength, $\alpha$ is the aperture angle, $I_{MAX}$ is the intensity maximum, and $I_{SAT}$ is the intensity of the saturated signal. Thus, efficient saturation of the signal is crucial for improved resolution.

The previous proof-of-concept work was done with a low repetition rate, high peak power laser. We chose this laser because the peak power provided a relatively higher likelihood of driving the depletion process, which becomes more effective as the depletion power is increased. However, the high peak power has a high likelihood of damaging soft matter samples. In order to adapt our technique for work with biological materials, we modified our initial technique to employ a MHz repetition rate laser, allowing us greater flexibility in the possible powers. While lower peak power decreases the signal magnitude per pulse, the increased number of pulses per

second allows for a higher rate of averaging. The increased range of possible powers allows us to use higher powers for proof-of-concept experiments with more robust samples and lower powers for imaging experiments on samples with a low damage threshold. In this paper, we discuss adapting our super-resolution SRS technique on a MHz laser system. We address detection schemes and optimizing depletion efficiency. We also demonstrate sub-diffraction limit resolution and discuss limitations to further resolution enhancement and applications to biological samples using this laser system.

## Methods

The experiments described herein utilized a Clark-MXR Impulse laser with a fundamental output at a central wavelength of 1035 nm and a manufacturer-specified pulse duration of 250 fs. A schematic of the setup is shown in **Figure 1**. The tunable repetition rate was set to 2.04 MHz and the output power was typically set to approximately 12 W. Using beam splitters, the fundamental output was split into three beams: the Raman pump and probe to generate the stimulated Raman signal, and the depletion beam to improve the spatial resolution. To create the Raman pump beam, 6 W of the output beam were sent through a grating filter.[50] This narrows the spectral bandwidth of the beam and broadens its temporal bandwidth. To create the white light continuum for the Raman probe beam, 3 W of the output beam were focused onto a 3 or 5 mm thick neodymium-doped yttrium aluminum garnet (Nd:YAG) crystal (Newlight Photonics) with a 75 mm focal length lens. The resulting beam was then passed through a prism compressor containing two SF10 prisms (Edmund Optics) separated by 39 in to remove the temporal chirp inherent in the continuum generation process.[51] In the prism compressor, wavelengths shorter than 1035 nm were filtered with a beam block. The remaining bandwidth extended to

approximately 1500 nm. The remaining 3 W of the fundamental were used for the depletion beam. To generate the depletion beam's toroidal spatial profile, the beam was passed through a vortex phase plate (RPC Photonics, VPP-1a). The diameter of each beam was optimized with a 2:1 telescope.

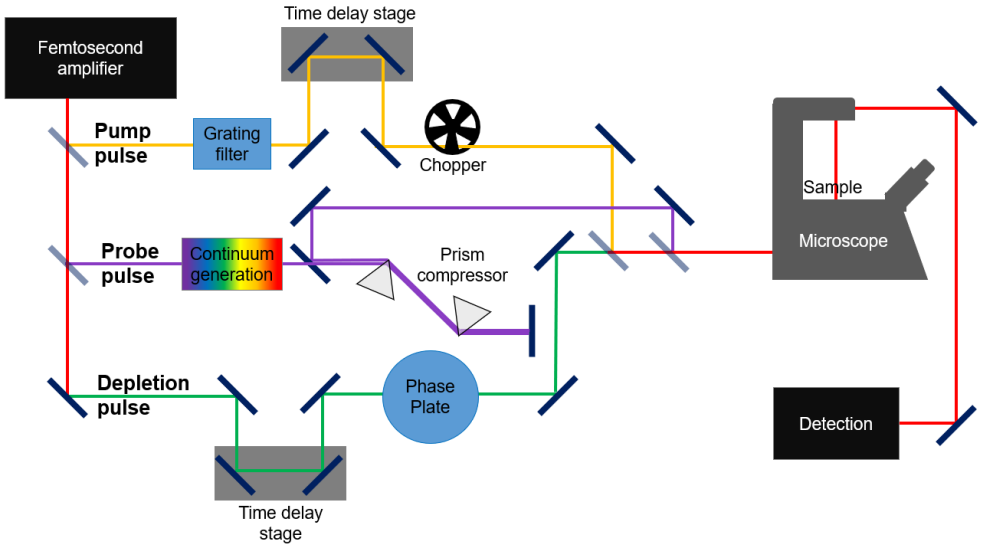


**Figure 1.** Experimental setup for sub-diffraction limit SRS imaging with a MHz laser. The Raman pump, Raman probe, and depletion pulses are overlapped spatially and temporally at the microscope sample position. Signal is collected in a transmission geometry and detected by an InGaAs photodiode array or a single-channel photodiode with lock-in amplification.

Initial signal-to-noise experiments were performed without the depletion beam or a microscope. For these experiments, the Raman pump and Raman probe were focused colinearly onto the sample with a 100 mm focal length achromatic lens and the signal was collected with a 60 mm focal length lens after the sample. In all remaining experiments, the three slightly noncolinear beams were sent into the back aperture of an inverted microscope (Olympus IX-73). The beams were focused onto the sample using one of several objectives and were collimated using a condenser with an NA of 0.55 (Olympus, IX2-LWUCD). In either sample setup, following signal collimation the Raman pump was filtered out with a 1064 RazorEdge filter (Semrock). The

Raman probe and SRS signal were then focused through a slit into a spectrograph (Princeton Instruments, 2300i) using a 100 mm focal length achromatic lens.

Multiple schemes were used to detect the SRS signal. Unless otherwise noted, the experiments were performed using single-element detection with an InGaAs photodiode (Thorlabs, DET10C) and a lock-in amplifier (Stanford Research Systems, SR830) with a time constant of 30 ms. For these experiments, a mirror was placed in the dispersed beam path in the spectrograph, reflecting a narrow range of the spectrum through a slit and onto the single-element photodiode. The Raman pump was typically modulated at a frequency of 997 Hz with a chopper wheel (Thorlabs). For the signal-to-noise data shown in **Figure 2b**, the Raman pump was modulated at a frequency of 953 Hz. Data was collected via home-written LabVIEW programs. For initial alignment and signal-to-noise comparisons, a 1024-pixel InGaAs photodiode array (Princeton Instruments, PyLoN-IR: 1024-1.7) cooled by liquid nitrogen was used, and data was collected using LightField (Princeton Instruments).

A 2 mm cuvette was filled with neat benzene for depletion efficiency experiments. Imaging experiments were performed on a 200 μm-thick piece of diamond formed by chemical vapor deposition purchased from Diamond Materials GMBH. The diamond was sandwiched between a 1 mm thick glass microscope slide and a 0.17 mm thick coverslip for protection.

**Results and Discussion**

We began by establishing reproducible SRS signal using the new setup. For initial experiments, we implemented a broadband detection scheme using a photodiode array in order to take advantage of the broad spectral bandwidth of the Raman probe pulse. This allows for a wide range of potential vibrations to be observed simultaneously, as opposed to narrowband SRS in

which the wavelength of one of the pulses must be tuned such that the difference in energy between the Raman pump and probe pulses equals the energy required to excite a given vibrational mode. Benzene was chosen as our model sample due to its large Raman cross section. The signal is displayed as Raman gain to normalize the intensity of the peaks due to the varying probe intensity across the spectral window.[52] This is calculated using the following equation:

$$Raman\ gain = \frac{Probe\ spectrum\ with\ pump\ on}{Probe\ spectrum\ with\ pump\ off} \quad (1)$$

The resulting spectrum, showing multiple peaks, can be seen in **Figure 2a**. While the signal magnitude observed here is reasonable, there is also a high level of noise in the detected probe spectra, which is evident in the sloping, noisy background. The probe noise necessitates the use of long averaging, which becomes especially relevant for materials with lower Raman scattering cross sections. In order to avoid either prohibitively long acquisition times or high pulse powers that would damage soft matter samples, achieving the highest possible signal-to-noise ratio (SNR) is vital to the success of the technique.

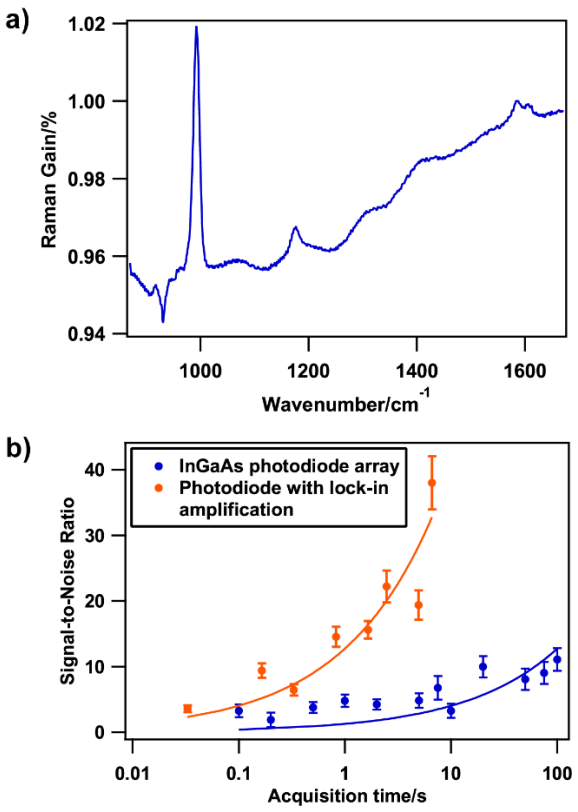


**Figure 2. (a)** Broadband stimulated Raman spectrum of liquid benzene collected using broadband detection with an InGaAs photodiode array. In this spectrum, 2000 acquisitions of a duration of 0.1 s each were averaged. The spectrum was smoothed using a 7 point Savitzky-Golay filter. The Raman pump power was set to 10 mW. **(b)** Comparison of the SNR between an InGaAs photodiode array and a single-element photodiode with lock-in amplification. For the data taken with the photodiode array, the Raman pump power was 84.3 mW. For the data taken using lock-in amplification, the Raman pump power was 101 mW. The spectra collected to calculate the lock-in amplification SNR data was acquired by scanning the monochromator grating, so the acquisition time for this data refers to the amount of time data was acquired for at each wavelength. Fits to square root functions are included to guide the eye. Error bars represent the errors in the peak amplitude fit values.

Lock-in amplification with a single channel photodiode offers an alternative detection scheme with potential for an improved SNR. It is performed by modulating the detected signal at a given wavenumber, then extracting the signal from the carrier wave, which filters out noise occurring at frequencies other than the modulation frequency. While it does improve SNR, it severely limits the detection bandwidth as an entire spectrum cannot be collected simultaneously

due to the cost of multiplexing. To evaluate whether the SNR improvement is worth the loss of detection bandwidth, we compared the SNR of our photodiode array to a single channel photodiode with lock-in amplification using spectra of the ring-breathing mode of benzene at 992 $cm^{-1}$. We calculated the SNR by dividing the fitted amplitude of the peak by the standard deviation of a portion of the background. While lock-in amplification detects just one wavenumber at a time, in these experiments we scanned the spectrometer grating so that a spectrum could be compiled. These data are shown in **Figure 2b**. As expected, the SNR using lock-in amplification was significantly improved over the photodiode array, by approximately an order of magnitude in our experiments. It is worth noting the acquisition time displayed on the x-axis for the lock-in amplification data refers to the acquisition time per wavelength, while the acquisition time for the InGaAs photodiode array refers to the acquisition time per spectrum. This allows for a more direct comparison between the two methods because scanning the grating is not done during imaging experiments. The spectrometer grating can be set such that the wavelength corresponding to an identifiable Raman-active vibration of the analyte of interest is detected by the photodiode at each position on the sample, eliminating the need for an entire spectrum. Although the advantage of using a broadband Raman probe pulse is diminished by the use of lock-in amplification, some benefits remain. The pulse wavelengths do not need to be retuned to match new wavenumbers, and if there are multiple wavenumbers of interest for a given analyte, additional lock-in amplifier channels can be used, making multiplex detection still possible using multiple photodiodes.[53]

In order to determine the system's viability for super-resolution SRS, we compared experiments performed with this higher repetition rate laser to the proof-of-concept results obtained by Silva et al. with a 1 kHz laser system.[20] For these experiments, a Gaussian-shaped

depletion beam was used in order to investigate the fundamental relationship between the addition of the depletion pulse and the depletion efficiency. **Figure 3a** directly shows effective depletion of the ring-breathing mode of benzene with an efficiency of 62%. **Figure 3b** shows the depletion efficiency as a function of laser polarization of the depletion beam. As expected, the signal is most efficiently depleted when the polarization of the depletion beam matches that of the Raman pump and Raman probe, and depletion is low when the depletion beam is perpendicularly polarized relative to the other beams. These results are congruent with the findings by Silva et al., although the maximum depletion achieved with the MHz laser system is lower overall.[20]

We scanned the beams over the edge of a 200 μm-thick chemical vapor deposition-prepared diamond plate to compare to the resolution enhancement seen with the 1 kHz setup. Here, we used a toroidal depletion beam to deplete the Raman signal in a spatially defined area. The resulting scan can be seen in **Figure 3c**. We calculated the resolution of the line scans by fitting the Raman amplitude of the 1332 $cm^{-1}$ diamond peak vs the sample position to a logistic function (equation 2).

$$y = \frac{A}{1+e^{\frac{x_0-x}{\sigma}}} \tag{2}$$

The parameter σ, which describes the growth rate of the function, gives the spatial resolution achieved when multiplied by 3.33.[54] We calculated the diffraction limit to be 1.76 μm from the wavelength and numerical aperture of the system using the Rayleigh criterion.[55] In this case, the spatial resolution improved from 3.1 ± 0.3 μm without the depletion beam to 1.5 ± 0.5 μm with it, meaning sub-diffraction limit spatial resolution was achieved. Although the spatial resolution was not at the diffraction limit without the depletion beam, likely due to the thickness of the sample and the beams not perfectly backfilling the objective,[56] the depletion beam improved the spatial resolution by 52%, which was similar to that found with the 1 kHz laser setup.[20] It is noteworthy

that the data with the depletion beam on is noisier than the data with the depletion beam off. This is due to cross-phase modulation (XPM) induced by the depletion beam. XPM occurs when a high intensity beam causes the refractive index of a material to change, which in turn changes the phase of other beams interacting with the material.

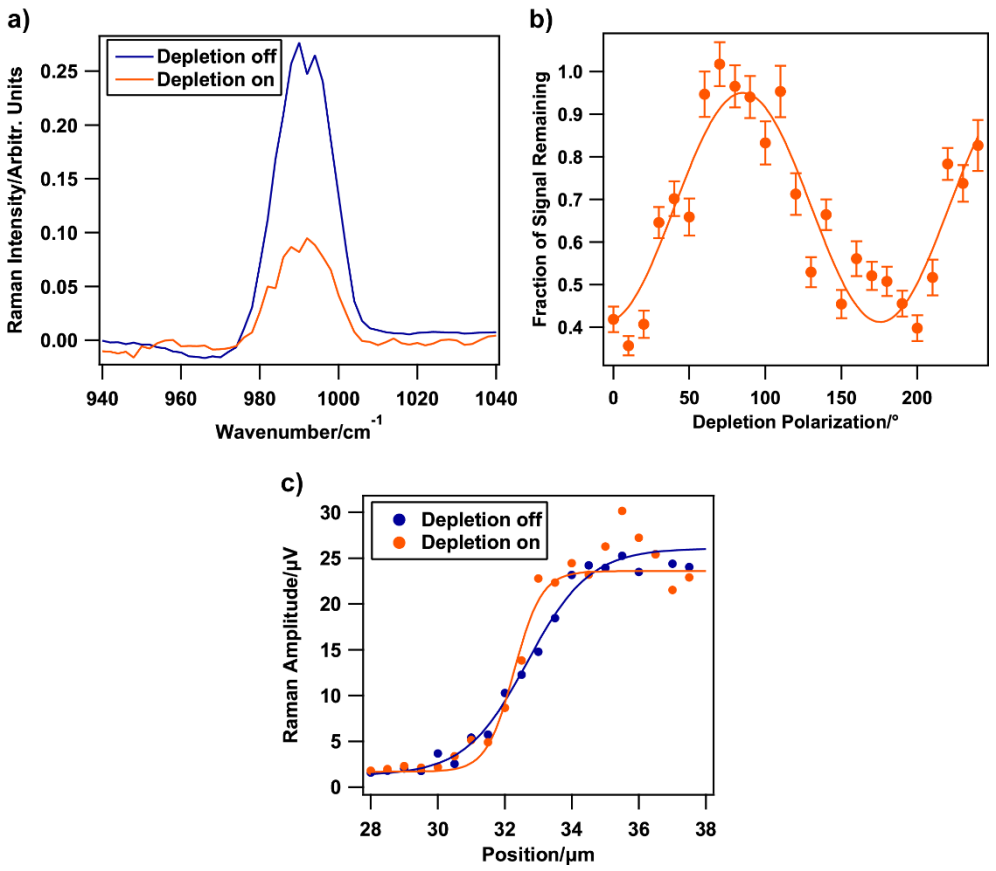


**Figure 3**. Demonstrating the photophysical properties of depletion using a MHz repetition rate laser and lock-in amplification. **(a)** This spectrum shows approximately 64% depletion of the stimulated Raman signal of the ring-breathing mode in a sample of liquid benzene. **(b)** The depletion efficiency vs. the polarization of the depletion beam was measured in the ring-breathing mode of benzene. The depletion beam polarization was set using a half waveplate. Error bars represent the propagated errors in the peak amplitude fit values. For **(a)** and **(b)**, the Raman pump power was 80.8 mW, the Raman probe power was 22.5 mW, the depletion power was 368 mW, and a Gaussian-shaped depletion beam was used. **(c)** Improved spatial resolution by 52% demonstrated by a line scan across the edge of a 200 μm thick diamond plate using a toroidal depletion beam. A 10x objective with an NA of 0.25 was used as the focusing optic. The Raman pump power was 149 mW, the Raman probe power was 5 mW, and the depletion power was 295 mW.

While a resolution enhancement of 52% is a promising result, further improvement is required to achieve true super-resolution comparable to that of fluorescence-based techniques. Since the depletion beam itself is diffraction limited, a nonlinear relationship between depletion power and depletion efficiency is required to achieve spatial resolution on the desired length scales.[57] **Figure 4a** shows the signal depletion of the benzene ring-breathing mode vs the power of the depletion beam, which was Gaussian-shaped for this experiment. While the desired nonlinear relationship was demonstrated with 1 kHz setup,[20] the relationship demonstrated using the MHz setup was less compelling, as **Figure 5** shows a roughly linear relationship between the two. We previously showed on the kHz system that 97% depletion is easily achievable, although with significant sample damage. The depletion of ~50% achieved here is mainly limited by noise in the laser source. As such, we were unable to obtain further improvements in the spatial resolution beyond what is shown in **Figure 3c**.

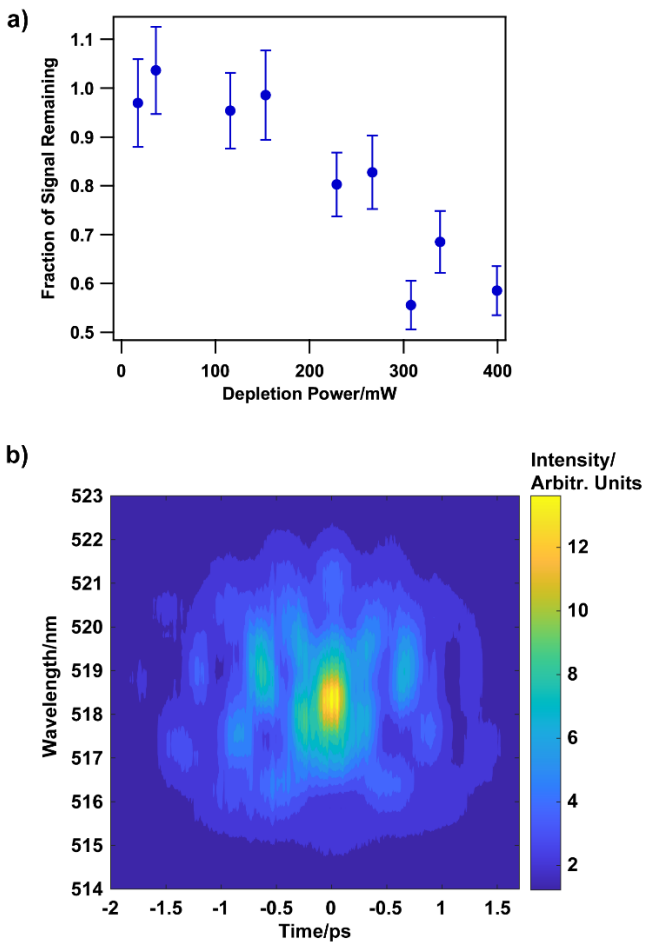


**Figure 4. (a)** Depletion of the stimulated Raman signal of the ring-breathing mode of benzene vs depletion beam power. The Raman pump power was 106.2 mW and the Raman probe power was 33.2 mW. Error bars represent the propagated errors in the peak amplitude fit values. **(b)** FROG data showing fundamental laser output intensity as a function of time and wavelength for the MHz setup. The pulse profile deviates from the desired 2D Gaussian shape.

One possible explanation for less efficient depletion could be the laser pulse durations. The output pulses from the laser used in the MHz setup were factory-specified to be 250 fs, compared to 90 fs in the setup using the 1 kHz laser system. Experiments carried out on the 1 kHz laser setup indicate that depletion is most efficient when the peak of the depletion pulse is temporally overlapped with the peaks of the Raman pump and probe pulses.[20] It is possible that the depletion process could not be driven as efficiently as expected at a given average power on the MHz setup

when compared to the 1 kHz setup because the depletion pulse energy was more broadly distributed temporally on the MHz setup, resulting in lower peak fluence values. We used a home-built frequency-resolved optical gating (FROG) apparatus to further investigate the pulse profile.[58] **Figure 4b** shows the FROG trace of the fundamental output of the MHz laser. It is clear that the intensity profile is inconsistent and deviates from the expected Gaussian shape in both the time and energy domains. Any behavior that does not follow a 2D Gaussian profile also indicates phase inconsistencies.

These results indicate that an erratic, noisy pulse profile makes efficient depletion of the SRS signal difficult, and hinders application of this system to biological samples. We posit that, due to the sensitive nonlinear optical processes that drive the depletion of the SRS signal, fluctuations in the phase, duration, or intensity of the pulses lead to inconsistent and inefficient depletion. Therefore, ultrashort pulses with a well-defined temporal profile are required. We expect this is especially true for SRS with a broadband fs probe beam. As the duration of our probe pulse is very short, all vibrational coherences are created in a narrow time window. A depletion pulse that is also very short is therefore able to most efficiently deplete those vibrational coherences, as less of the depletion power is wasted in the time before the coherences are created. Additionally, a depletion pulse with a well-defined phase and polarization profile is also vital, as the data in **Figure 3b** demonstrates. Given the inconsistencies observed in the pulse profile in **Figure 4b**, it is unsurprising that depletion of SRS was inconsistent and further improvements in spatial resolution were not observed. It is likely that regular adjustments to the MHz laser, in particular changing the repetition rate so that different experiments could be performed, put added strain on the amplifier fiber and contributed to the inconsistent pulse. Additionally, the distance

between amplifier output and the samples was quite long in our setup. Shortening it may also help improve the stability of the pulse. Work is ongoing into the processes contributing to the depletion of the SRS signal. A better understanding of this will allow us to optimize experiments to maximize depletion.

## Conclusion

Here, we discuss the adaptation of super-resolution SRS for a MHz laser system with the goal of mitigating damage to soft materials while further enhancing spatial resolution. We demonstrated depletion of the SRS signal, and depletion beam polarization results were in good agreement with previous work utilizing a 1 kHz laser system.[20] Additionally, diamond imaging experiments resulted in an improvement in spatial resolution by 52% leading to sub-diffraction limit resolution, which was similar to results obtained with a 1 kHz laser. However, depletion efficiency as a function of depletion beam power did not scale as observed previously, and we did not produce further improvements in resolution. This was likely due to the inconsistent shape and long duration of the fundamental laser output from the MHz system. These results highlight the importance of reliable and stable pulses in driving sensitive nonlinear optical processes.

## Acknowledgements

Funding for this work was provided by the National Science Foundation, Grant CHE-1552849 (C.T.G.) and the National Institutes of Health, Grant 5R35-GM119441 (D.P. and M.J.L.). C.T.G. acknowledges the Torske Klubben Fellowship for support, D.P. acknowledges postdoctoral funding from the Ford Foundation, and M.J.L. acknowledges the NSF GRFP for support. This

paper is dedicated to the memory of Rick Van Duyne, who was an inspiration for this project and was always excited about pushing the limits of Raman spectroscopy.

## References


[1] S. W. Hell, J. Wichmann, *Opt. Lett.* **1994**, *19*, 780.

[2] E. Betzig, G. H. Patterson, R. Sougrat, O. W. Lindwasser, S. Olenych, J. S. Bonifacino, M. W. Davidson, J. Lippincott-Schwartz, H. F. Hess, *Science* **2006**, *313*, 1642.

[3] M. J. Rust, M. Bates, X. Zhuang, *Nat. Methods* **2006**, *3*, 793.

[4] C. T. Graefe, D. Punihaole, C. M. Harris, M. J. Lynch, R. Leighton, R. R. Frontiera, *Anal. Chem.* **2019**, *91*, 8723.

[5] S. J. Sahl, S. W. Hell, S. Jakobs, *Nat. Rev. Mol. Cell Biol.* **2017**, *18*, 685.

[6] Z. Liu, L. D. Lavis, E. Betzig, *Mol. Cell* **2015**, *58*, 644.

[7] J. Tønnesen, G. Katona, B. Rózsa, U. V. Nägerl, *Nat. Neurosci.* **2014**, *17*, 678.

[8] A. Szymborska, A. de Marco, N. Daigle, V. C. Cordes, J. A. G. Briggs, J. Ellenberg, *Science* **2013**, *341*, 655.

[9] K. Xu, G. Zhong, X. Zhuang, *Science* **2013**, *339*, 452.

[10] Y. M. Sigal, R. Zhou, X. Zhuang, *Science* **2018**, *361*, 880.

[11] L. Große, C. A. Wurm, C. Brüser, D. Neumann, D. C. Jans, S. Jakobs, *EMBO J.* **2016**, *35*, 402.

[12] R. Salvador-Gallego, M. Mund, K. Cosentino, J. Schneider, J. Unsay, U. Schraermeyer, J. Engelhardt, J. Ries, A. J. García-Sáez, *EMBO J.* **2016**, *35*, 389.

[13] M. J. Skaug, M. L. Longo, R. Faller, *J. Phys. Chem. B* **2011**, *115*, 8500.

[14] S. L. Veatch, S. S. W. Leung, R. E. W. Hancock, J. L. Thewalt, *J. Phys. Chem. B* **2007**,

*111*, 502.

[15] L. Greenbaum, R. Chana, L. Ronit, M. Zvi, *Biol. Chem.* **2000**, *381*, 1251.

[16] T. Bernas, M. Zarębski, R. R. Cook, J. W. Dobrucki, *J. Microsc.* **2004**, *215*, 281.

[17] P. P. Laissue, R. A. Alghamdi, P. Tomancak, E. G. Reynaud, H. Shroff, *Nat. Methods* **2017**, *14*, 657.

[18] H. Tsurui, H. Nishimura, S. Hattori, S. Hirose, K. Okumura, T. Shirai, *J. Histochem. Cytochem.* **2000**, *48*, 653.

[19] T. Niehörster, A. Löschberger, I. Gregor, B. Krämer, H.-J. Rahn, M. Patting, F. Koberling, J. Enderlein, M. Sauer, *Nat. Methods* **2016**, *13*, 257.

[20] W. R. Silva, C. T. Graefe, R. R. Frontiera, *ACS Photonics* **2016**, *3*, 79.

[21] W. P. Beeker, P. Groß, C. J. Lee, C. Cleff, H. L. Offerhaus, C. Fallnich, J. L. Herek, K.-J. Boller, *Opt. Express* **2009**, *17*, 22632.

[22] W. Liu, H. Niu, *Phys. Rev. A* **2011**, *83*, 023830.

[23] C. Cleff, P. Groß, C. Fallnich, H. L. Offerhaus, J. L. Herek, K. Kruse, W. P. Beeker, C. J. Lee, K.-J. Boller, *Phys. Rev. A* **2013**, *87*, 033830.

[24] D. Wang, S. Liu, Y. Chen, J. Song, W. Liu, M. Xiong, G. Wang, X. Peng, J. Qu, *Opt. Express* **2017**, *25*, 10276.

[25] A. Gasecka, A. Daradich, H. Dehez, M. Piché, D. Côté, *Opt. Lett.* **2013**, *38*, 4510.

[26] T. Würthwein, N. Irwin, C. Fallnich, *J. Chem. Phys.* **2019**, *151*, 194201.

[27] V. Raghunathan, E. O. Potma, *J. Opt. Soc. Am. A* **2010**, *27*, 2365.

[28] H. Kim, G. W. Bryant, S. J. Stranick, *Opt. Express* **2012**, *20*, 6042.

[29] S. Rieger, M. Fischedick, K.-J. Boller, C. Fallnich, *Opt. Express* **2016**, *24*, 20745.

[30] S. Rieger, T. Würthwein, K. Sparenberg, K.-J. Boller, C. Fallnich, *J. Chem. Phys.* **2018**,

*148*, 204110.

[31] L. Gong, H. Wang, *Phys. Rev. A* **2014**, *90*, 013818.

[32] D. Kim, D. S. Choi, J. Kwon, S.-H. Shim, H. Rhee, M. Cho, *J. Phys. Chem. Lett.* **2017**, *8*, 6118.

[33] D. S. Choi, B. J. Rao, D. Kim, S.-H. Shim, H. Rhee, M. Cho, *Phys. Chem. Chem. Phys.* **2018**, *20*, 17156.

[34] M. Cho, *J. Chem. Phys.* **2018**, *148*, 014201.

[35] L. Wei, F. Hu, Z. Chen, Y. Shen, L. Zhang, W. Min, *Acc. Chem. Res.* **2016**, *49*, 1494.

[36] M. S. Messina, C. T. Graefe, P. Chong, O. M. Ebrahim, R. S. Pathuri, N. A. Bernier, H. A. Mills, A. L. Rheingold, R. R. Frontiera, H. D. Maynard, A. M. Spokoyny, *Polym. Chem.* **2019**, *10*, 1660.

[37] D. Punihaole, R. J. Workman, S. Upadhyay, C. Van Bruggen, A. J. Schmitz, T. M. Reineke, R. R. Frontiera, *J. Phys. Chem. B* **2018**, *122*, 9840.

[38] Y. Wang, R. Purrello, S. Georgiou, T. G. Spiro, *J. Am. Chem. Soc.* **1991**, *113*, 6368.

[39] N. S. Myshakina, Z. Ahmed, S. A. Asher, *J. Phys. Chem. B* **2008**, *112*, 11873.

[40] D. Punihaole, R. S. Jakubek, E. M. Dahlburg, Z. Hong, N. S. Myshakina, S. Geib, S. A. Asher, *J. Phys. Chem. B* **2015**, *119*, 3931.

[41] T. Miura, H. Takeuchi, I. Harada, *J. Raman Spectrosc.* **1989**, *20*, 667.

[42] D. Punihaole, R. S. Jakubek, R. J. Workman, S. A. Asher, *J. Phys. Chem. Lett.* **2018**, *9*, 1944.

[43] L. Wei, Z. Chen, L. Shi, R. Long, A. V Anzalone, L. Zhang, F. Hu, R. Yuste, V. W. Cornish, W. Min, *Nature* **2017**, *544*, 465.

[44] R. C. Prince, R. R. Frontiera, E. O. Potma, *Chem. Rev.* **2017**, *117*, 5070.

[45] B. G. Saar, C. W. Freudiger, J. Reichman, C. M. Stanley, G. R. Holtom, X. S. Xie, *Science* **2010**, *330*, 1368.

[46] C. W. Freudiger, W. Min, B. G. Saar, S. Lu, G. R. Holtom, C. He, J. C. Tsai, J. X. Kang, X. S. Xie, *Science* **2008**, *322*, 1857.

[47] P. Nandakumar, A. Kovalev, A. Volkmer, *New J. Phys.* **2009**, *11*, 33026.

[48] Y. Ozeki, W. Umemura, Y. Otsuka, S. Satoh, H. Hashimoto, K. Sumimura, N. Nishizawa, K. Fukui, K. Itoh, *Nat. Photonics* **2012**, *6*, 845.

[49] S. W. Hell, *Science* **2007**, *316*, 1153.

[50] S. Shim, R. A. Mathies, *Appl. Phys. Lett.* **2006**, *89*, 121124.

[51] R. L. Fork, O. E. Martinez, J. P. Gordon, *Opt. Lett.* **1984**, *9*, 150.

[52] P. Kukura, D. W. McCamant, R. A. Mathies, *Annu. Rev. Phys. Chem.* **2007**, *58*, 461.

[53] K. Seto, Y. Okuda, E. Tokunaga, T. Kobayashi, *Rev. Sci. Instrum.* **2013**, *84*, 83705.

[54] A. E. Curtin, R. Skinner, A. W. Sanders, *Microsc. Microanal.* **2015**, *21*, 771.

[55] Rayleigh, *London, Edinburgh, Dublin Philos. Mag. J. Sci.* **1879**, *8*, 261.

[56] R. L. McCreery, *Raman Spectroscopy for Chemical Analysis*, John Wiley & Sons, Inc., New York, **2000**.

[57] B. Harke, J. Keller, C. K. Ullal, V. Westphal, A. Schönle, S. W. Hell, *Opt. Express* **2008**, *16*, 4154.

[58] R. Trebino, K. W. DeLong, D. N. Fittinghoff, J. N. Sweetser, M. A. Krumbügel, B. A. Richman, D. J. Kane, *Rev. Sci. Instrum.* **1997**, *68*, 3277.